Marine Geology 440 (2021) 106569

Contents lists available at ScienceDirect

Marine Geology

journal homepage: www.elsevier.com/locate/margo

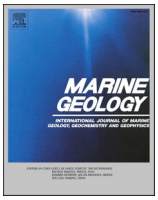

On the mechanism behind the shift of the turbidity maximum zone in response to reclamations in the Yangtze (Changjiang) Estuary, China

Lizhi Teng [a], Heqin Cheng [a,b,*], H.E. de Swart [c], Ping Dong [d], Zhanhai Li [a], Jiufa Li [a], Yajun Wang [a]

[a] State Key Laboratory of Estuarine and Coastal Research, East China Normal University, Shanghai 200241, China
[b] Institute of Eco-Chongming, East China Normal University, Shanghai 202162, China
[c] Institute for Marine and Atmospheric Research, Utrecht University, Princetonplein 5, 3584 CC Utrecht, the Netherlands
[d] School of Engineering, University of Liverpool, Liverpool L69 3GH, UK

ARTICLE INFO

Keywords:
Suspended sediment
Estuarine engineering
Channel geometry
Remote sensing images

ABSTRACT

Reclamation in estuaries can greatly change the channel geometry and hydrodynamic conditions and these changes may have significant impacts on spatial and temporal distribution of the turbidity maximum zone. This study focuses on the effects of a large area of reclamation built in 2007–2018 and the behavior of the turbidity maximum zone along the North Channel of the Yangtze Estuary. Data were collected of bathymetry in the North Channel, tidal elevations at Sheshan Station, river discharge at Datong Station and turbidity, retrieved from six Landsat remote sensing images in the dry season from 2006 to 2019. In-situ measured data on flow velocity and suspended sediment concentration were obtained in the dry season of 2003 and 2018. Analysis of the data revealed that reclamations, which led to narrowing (0.86–2.74 km) and fixing of the channel, caused erosion of 0.19–3.72 m in the deep channel and deposition on the tidal flats. Furthermore, it was found that the length of the turbidity maximum zone decreased: its landward boundary shifted 5 km seaward during spring tide and 17 km seaward during neap tide in the dry season. The position of the seaward boundary wandered within a range of 3 km, being further downstream during neap tide than that during spring tide. A conceptual model of changes in the borders of the turbidity maximum zone in response to reclamation is proposed. After the reclamation works, the deeper and narrower channel intensified ebb-dominance of the flow velocity. The coarsening of bed sediment weakened resuspension and decreased the bottom tidally averaged suspended sediment concentration. These changes led to a significant decline in the depth-mean of tidally averaged suspended sediment concentration and caused the seaward movement of the landward boundary of the turbidity maximum zone.

1. Introduction

The turbidity maximum zone (TMZ) is the region within an estuary where the suspended sediment concentration (SSC) is significantly higher than that in adjacent waters. The TMZ is formed as a result of sediment accumulating under the dynamic interaction between runoff, stratification and tides and it regularly migrates within a certain range (Li and Zhang, 1998; Doxaran et al., 2009). The dynamics of suspended sediment in the TMZ plays an important role in the morphological evolution of the channel and shoals (Wu et al., 2012), as well as in the transport of nutrients and pollutants (Gebhardt et al., 2005). The TMZ has been observed and studied in many estuaries around the world (Burchard et al., 2018 and references herein) and measurements of its spatial distribution are often used as a reference for maintaining navigation channels (de Jonge et al., 2014) and for ecological conservation (Mitchell, 2013).

It is well established that land reclamation projects conducted in estuaries modify the channel geometry and alter the hydrodynamics and accumulation of sediment (Williams et al., 2015; Gao et al., 2018). For example, the tidal-choking effect of reclamation caused a decrease in flood dominance within the main branch of the Yalu River Estuary (Cheng et al., 2020) and reclamation in the Ems estuary decreased the area of subtidal flats by reducing the amount of fine-grained sediment deposited (van Maren et al., 2016). However, the effect of reclamation on changes in the characteristics of the TMZ, such as shifts of its borders and location and intensity of the maximum SSC, has hardly been

* Corresponding author at: State Key Laboratory of Estuarine and Coastal Research, East China Normal University, Shanghai 200241, China.
E-mail address: hqch@sklec.ecnu.edu.cn (H. Cheng).

https://doi.org/10.1016/j.margeo.2021.106569
Received 31 December 2020; Received in revised form 1 June 2021; Accepted 13 July 2021
Available online 22 July 2021

studied. A series of reclamation projects has been conducted in the Yangtze Estuary (YE) since the 1990s. During this period, the land area in the YE has increased by 10% (Zhang et al., 2020), the growth rate of the subtidal zone has decreased from 6.0 $km^2\ yr^{-1}$ (1977–1994) to −6.2 $km^2\ yr^{-1}$ (1994–2011) (Du et al., 2016), and the slope of tidal flats between the −2 m and −3 m isobaths has become steeper (Wei et al., 2017). Most notably the channel geometry of the North Channel (NC) of the YE has been strongly modified over the past two decades by reclamation projects, such as the Qingcaosha Reservoir and the Hengsha East Shoal Promoting Siltation project (HESP) (Wu et al., 2016). Only minor artificial dredging takes place in the NC, so variations in geometry of the NC prior to reclamation works can be regarded as being natural (Mei et al., 2018). This makes the NC a suitable area to study the spatial change mechanism of the TMZ in response to estuarine reclamation.

The specific aims of this study are to quantify and explain, in the case of the NC, how reclamation changed 1) erosion-deposition patterns, 2) the length of the TMZ, both during spring and neap tides, 3) the flow, in particular its ebb/flood dominance, 4) the tidally averaged suspended sediment concentrations and 5) the composition of the bed sediment. The focus was on the dry season, as in the Yangtze River basin there have been minimal changes in the river discharge during that season since the Three Gorges Project and construction of fresh water reservoirs were completed (Guo et al., 2018).

Changes in channel morphology due to reclamations were derived from bathymetric data. Clearly, in-situ observations are most useful to assess variations in hydrodynamics and sediment dynamics between pre- and post-engineering. However, due to the lack of spatial coverage they cannot provide a macro view of the surface suspended sediment concentration (SSSC) distribution. Therefore, this study also uses remote sensing data of suitable spatial coverage at various time intervals (Wackerman et al., 2017). In the analyses conducted in this study, both Landsat remote sensing images and in situ measured data from the dry season were used. Combined with the spatial changes of TMZ and the variations of hydrodynamics and sediment dynamics between pre- and post-reclamations, the mechanism behind the shift of the TMZ in response to reclamation was unraveled.

The remainder of this paper is organized as follows. Section 2 introduces the geographical setting of the NC, including the information about the large-scale estuarine reclamation projects conducted in the NC over the past two decades. The methods used are presented in Section 3. Next, Section 4 describes the variations in channel geometry and spatial distribution of the TMZ of the NC post-reclamation. It further presents

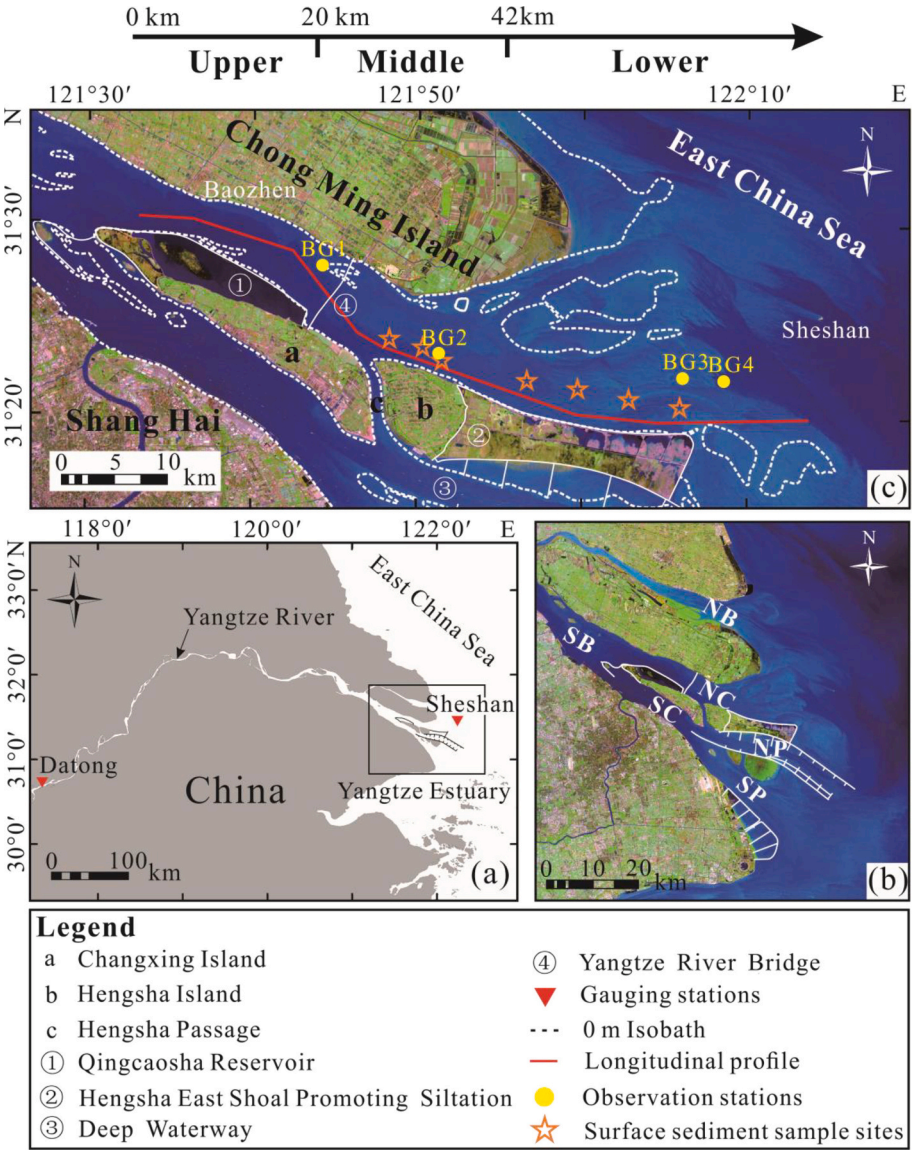

Fig. 1. Map showing the study area, with in (a) the location of Yangtze Estuary in China and the locations of Datong and Sheshan gauging stations; (b) Yangtze Estuary; (c) North Channel.

the changes in the hydrodynamic and vertical profiles of the tidally averaged suspended sediment concentration in the NC, as well as a grain size analysis of bed sediments. Section 5 discusses the spatial changes mechanism of the TMZ in response to reclamation in estuaries and proposes a conceptual model. Finally, Section 6 presents the conclusions.

2. Geographical setting

The Yangtze River has a length of approximately 6300 km. The YE is a mesotidal estuary (Luan et al., 2016) with a length of 90 km, a width of 90 km at its outer limit (Fig. 1b). Tidal range in the YE is in the range 2–3.83 m (Cheng et al., 2018). The annual average runoff between 2009 and 2019 was 8.89×10^{11} m^3 and observational data from Datong gauging station show that the annual average sediment transport decreased from 4.22×10^8 t yr^{-1} (2003–2019) to 1.32×10^8 t yr^{-1} (2003–2019) (Zheng et al., 2018). The YE has developed a three-order bifurcation and four-outlet configuration downstream. First, the YE is divided into North Branch (NB) and South Branch (SB) by Chong Ming Island. The South Branch is further divided into the North Channel (NC) and South Channel (SC) by Changxing and Hengsha Island. The South Channel is followed by the North Passage (NP) and South Passage (SP), which are separated by the Jiuduansha shoal (Fig. 1b). The NC is part of the second-order bifurcation with a length of 70 km (Wang et al., 2013). Approximately 50% of the runoff from the Yangtze River flows through the NC in the YE into the East China Sea (Wu et al., 2016).

The dates and locations of major engineering projects are shown in Table 1, from which it is evident that most of these projects began in 2005 and 2007. According to the magnitude of the tidal flow and the location of the project, the NC is divided into three segments (Fig. 1c). The upper segment is located near the Qingcaosha Reservoir, where runoff is strong. The middle segment is situated downstream of the Qingcaosha Reservoir. Finally, the lower segment is located near the Hengsha Shoal (HESP), where the effect of tidal flow is largest.

3. Materials and methods

3.1. Bathymetric data and variations in channel morphology

Bathymetric data of the NC between Baozhen and the outer estuary of the NC (Fig. 1c) were obtained from navigation maps compiled by the China Maritime Safety Administration (China MSA) in 1995, 2007 and 2018. These navigation maps have a scale of 1:25000 and the base levels provided are the theoretical depth datum, which is the lowest water level obtained from a combination of 13 gauging stations within the YE.

After geometric correction of navigation maps, shoreline and bathymetry data were transformed into a Universal Transverse Mercator Grid System (UTM) via the WGS84 coordinate system in ArcGIS. Digital elevation models (DEM) with a resolution of 200 m × 200 m were established through Kriging interpolation (e.g. Webster and Oliver, 2007). Deposition and erosion patterns during the period were then obtained by subtracting the previous morphological surveys. Positive values indicate depth reduced resulted from deposition, and vice versa. The large-scale reclamation projects, such as the Qingcaosha Reservoir and the HESP, both began in 2007. So the impact of reclamations on channel morphology could be analyzed based on the variations of deposition and erosion patterns between pre- and post-reclamations.

Table 1
Engineering built in NC during past three decades.

Engineering	Location	Time
Diversion port	Upper segment of NC	2007–2009
Qingcaosha Reservoir	Upper segment of NC	2005–2009
Shanghai Yangtze Bridge	Upper segment of NC	2005–2007
Reclamation on the north bank of Changxing Island	North bank of Changxing Island	2007–2009
Chongming East Shoal Reclamation	Chongming East Shoal	1998-
Hengsha East Shoal Promoting Siltation project	Hengsha East Shoal	2007-

3.2. Processing of remote sensing images and defining the TMZ

3.2.1. Selection of remote sensing images and estimating SSSC

The SSSC distributions in the years 2006 to 2019 within the YE were derived from remote sensing images obtained by Enhanced Thematic Mapper (ETM) of Landsat 7 with a spatial resolution of 30 m (Table 2).

The SSSC in the YE strongly differs between wet and dry seasons, spring and neap tides and between ebb and flood tides (Shen et al., 2013). To compare and analyze annual variations in the spatial distribution of the TMZ, we selected six remote sensing images that were similar in terms of the river discharge, the tide type and the time at which the images were taken.

Regarding river discharge, data were used from the Datong gauging station, which is located 600 km upstream of the YE (Fig. 1a) and is generally considered to be the landward boundary of tidal impact. It is the runoff and sediment inflow control station of the YE. This study used river discharge recorded at Datong Station on the same dates as that the remote sensing images were taken. Data about the tides (sea surface variations) for these dates were taken from the Sheshan gauging station. The latter is located outside the YE (Fig. 1a), where the tidal characteristics are less affected by reclamation projects (Cheng et al., 2018).

After precise geometric correction of the remote sensing images, the gray value, DN, of the original images was converted to radiance through radiometric calibration as

$$L = \text{gains} \times \text{DN} + \text{bias}$$

In this expression, L is the pixel radiance value of the remote sensing images and DN is the pixel gray. The value of the gains and bias were obtained from the header file of the remote sensing image. The FLASH module in ENVI software was used to correct the pixel radiance for influence from the atmosphere, which resulted in surface reflectance. The SSSC in the YE has obvious peaks in reflectance at band 4 (760–900 nm) and band 3 (630–690 nm) of the Landsat ETM and the fitting degree of the regression between the SSSC and the ratio of surface reflectance in these two bands (TM4/TM3) is high (Shen et al., 2013). Therefore, a linear regression equation was used to estimate the SSSC based on the surface reflectance of ETM bands 3 and 4,

$$SSSC = 2.2979x^2 - 2.2950x + 0.6206$$

where x is the ratio of surface reflectance of Landsat ETM bands 4 and 3 (TM4/TM3). The correlation between SSSC and the measured data is 0.92 and thus, use of this equation is effective in the YE (Shen et al., 2013).

Table 2
Six Landsat images from 2006 to 2019.

Serial number	Imaging data	Sensor	Mapping time (GMT)	Flow in Datong	Flood/Ebb	Tide type
a	2006-01-22	Landsat 7 ETM	02:14:56.50	16,800	Flood tide	Neap
b	2006-11-06	Landsat 7 ETM	02:14:49.55	16,800	Ebb tide	Spring
c	2011-02-05	Landsat 7 ETM	02:18:24.90	15,600	Flood tide	Spring
d	2013-12-11	Landsat 7 ETM	02:21:21.48	11,200	Ebb tide	Neap
e	2018-02-08	Landsat 7 ETM	02:26:35.25	17,700	Flood tide	Neap
f	2019-12-12	Landsat 7 ETM	02:06:56.02	11,100	Ebb tide	Spring

3.2.2. Definition of the TMZ

The area that has a significantly higher SSSC compared with the adjacent water in the inversion results of remote sensing images is called the TMZ (Doxaran et al., 2009). To make this more quantitative, it is important to realize that there are long-term trends in SSSC. Due to the retaining effect of large-scale projects in the basin, and particularly that of the Three Gorges Dam after 2003, there has been a continuous decrease in the sediment transport into the YE. This led to an overall reduction of the SSSC (Yang et al., 2010) and the area where SSSC is larger than 0.7 kg m^{-3} reduced by 23% (Jiang et al., 2013b). To avoid the influence of the overall reduction in SSSC on the determining the TMZ, the SSSC values derived from remote sensing images were converted into relative SSSC values (RSSSC) as

$$RSSSC = SSSC/ASSSC$$

Here, *ASSSC* is the area-averaged SSSC within the NC. TMZ is defined as the area where *SSSC* is larger than *ASSSC*, so where $RSSSC > 1$ As the TMZ of the YE is strongly affected by spring and neap tides (Jiang et al., 2013a, 2013b), the inversion results of remote sensing images in different years were divided into two groups (taken during spring and neap tide, respectively) to calculate the annual variation in the spatial distribution of the TMZ that occurred after completion of the reclamation projects.

3.3. Collection of hydrodynamic data and sediment concentration data

3.3.1. In-situ observations of flow velocity and suspended sediment concentration (SSC)

Vertical profiles of flow velocity and SSC during 25 h were continuously and synchronously observed in 2003 and 2018 (Fig. 1c and Table 3). Station BG1 was in the upper segment and station BG2 in the middle segment, station BG3 and BG4 were in the lower segment. They were used to assess the impact of reclamations on hydrodynamics and sediment dynamics. However, there was a lack of flow velocity profiles at station BG2 in 2003. The daily averaged tidal range was calculated as the average of four observed tidal ranges (two tidal cycles). Daily averaged wave heights during the times of observations were calculated from the dataset of European Centre for Medium-Range Weather Forecasts (ECMWF). During the different observation periods, wave conditions and river discharges were similar during spring tide and neap tide, respectively (Table 3). In tidal estuaries, the wind force potentially has a strong influence on estuarine circulation (Lange and Burchard, 2019; Zhang et al., 2019). Because wind speeds during observations were generally weak, the wind influence on circulation was not considered in this paper. The in-situ velocity data were obtained using an Acoustic Doppler Current Profiler (ADCP) fixed on one side of a boat using a steel fixing frame. Vertical profiles of turbidity were obtained every hour with an Optical Backscatter Sensor (OBS). The SSC at different depths was estimated according to the regression relation between the SSC and the turbidity obtained by the OBS calibrated in the laboratory.

The characteristics of surface sediment were obtained from samples (2 mm layer) along the main channel of the NC using a box dredger in April 2018 (Fig. 1c). The particle size distribution of the sediment was determined by using a laser particle size analyzer (LS13320) in the laboratory. The surface sediment was classified according to Folk et al. (1970).

3.3.2. The coefficient of flow dominance

Under the action of the longitudinal surface slope, the longitudinal density gradient and tidal mixing, there is significant estuarine circulation in the lower segment during the dry season. The residual current in the upper layer points seaward, whereas the lower layer residual current is directed landward. A large amount of sediment occurs in the area where landward and bottom flow meet, thereby forming the TMZ (Jiang et al., 2013a, 2013b; Li et al., 2019). The coefficient of flow dominance, *R*, reflects the degree of the ebb dominance in a tidal cycle under the same river discharge (Mei et al., 2018). The dominant flow coefficient *R* was calculated as

$$R = E/(E+F)$$

where *E* is the distance travelled by a particle during an ebb period and *F* the distance travelled by a water particle during flood tide:

$$E = \int_0^{T_E} V_E \cos\theta dt,$$

$$F = \int_0^{T_F} V_F \cos\theta dt.$$

Here, T_E and T_F are the ebb and flood period, V_E and V_F are the ebb and

Table 3
Date, location, tidal conditions, wave conditions, discharges in Datong and profiles.

Stations	Date	Distance from starting point(km)	Tidal condition	Discharge in Datong ($m^3 \cdot s^{-1}$)	Channel segment	Daily averaged tidal range (m)	Daily averaged wave height (m)	Profiles
BG1	2003-02-18	20	Spring tide	16,385	Upper	2.95	0.74–1.17	SSC profiles Velocity
	2003-02-24		Neap tide	21,000		1.43	0.55–0.86	profiles
BG2	2003-02-18	34	Spring tide	16,385	Middle	3.10	0.74–1.17	SSC profiles
	2003-02-24		Neap tide	21,000		1.32	0.55–0.86	
BG3	2003-02-18	56	Spring tide	16,385	Lower	3.05	0.74–1.17	SSC profiles Velocity
	2003-02-24		Neap tide	21,000		1.29	0.55–0.86	profiles
BG1	2018-04-18	20	Spring tide	17,300	Upper	3.64	0.73–0.98	SSC profiles Velocity
	2018-04-22		Neap tide	20,400		2.22	0.53–0.93	profiles
BG2	2018-04-18	34	Spring tide	17,300	Middle	2.94	0.73–0.98	SSC profiles Velocity
	2018-04-22		Neap tide	20,400		1.87	0.53–0.93	profiles
BG4	2018-04-18	65	Spring tide	17,300	Lower	2.92	0.73–0.98	SSC profiles Velocity
	2018-04-22		Neap tide	20,400		1.62	0.53–0.93	profiles

flood flow velocity and θ is the angle between the flow direction and the long axis direction of the tide. The flow is ebb-dominant when $R > 0.5$, otherwise it is flood-dominant. Note that V_E, V_F and θ are considered at different points on a vertical section.

The along-channel location where the coefficient of flow dominance near the bottom is 0.5 can be interpreted as the stagnation point of the near-bottom flow. In a previous study by Shen and Zhang (1992) it was already demonstrated that this stagnation point is close to the core of the TMZ. As the daily average discharges observed at Datong gauging station during the observations were similar in 2003 and 2018 (Table 3), the variations in the strengths of the ebb and flood flow could be analyzed by comparing the dominant flow coefficients in different years.

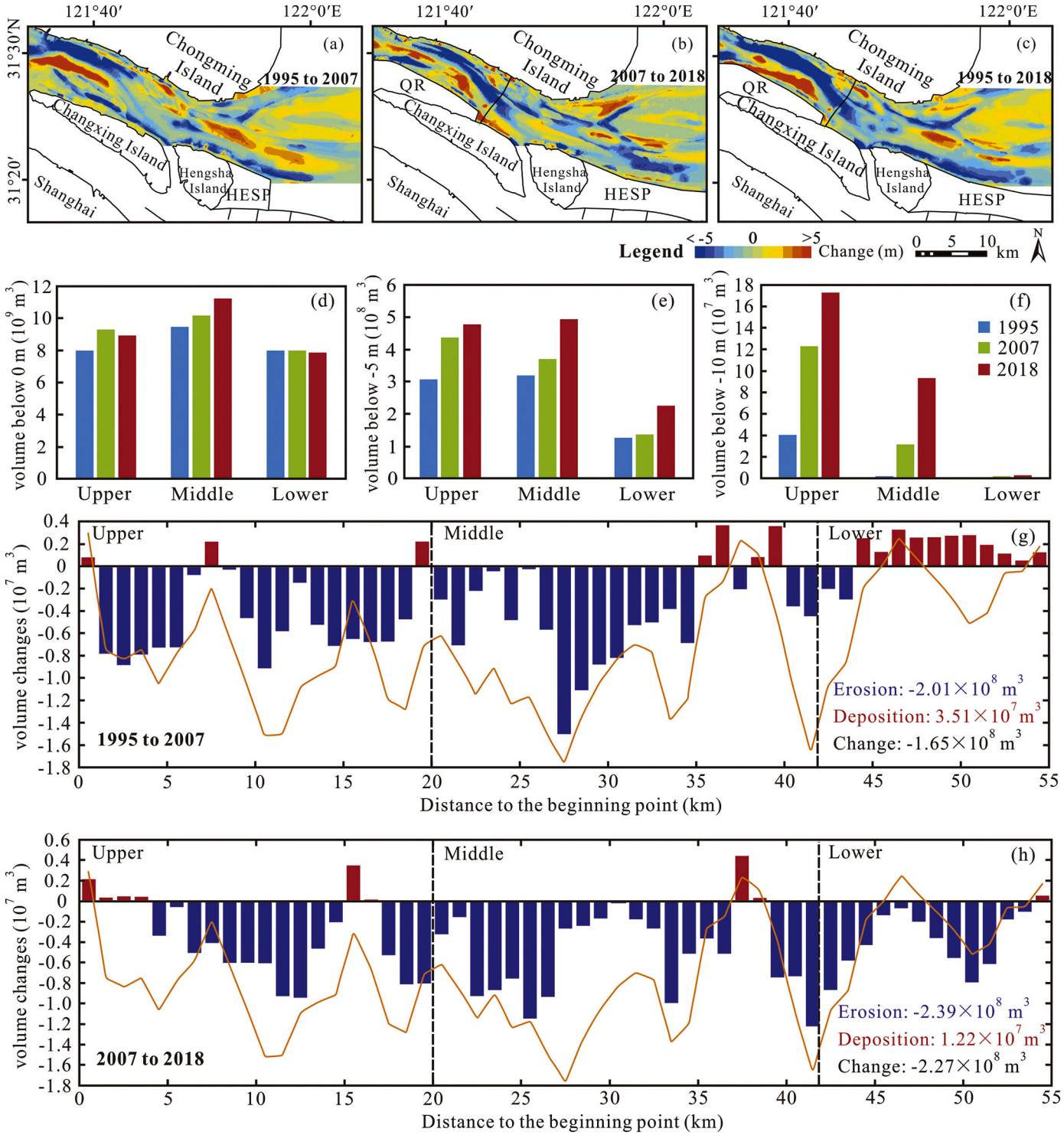

Fig. 2. Changes in erosion-deposition patterns of North Channel, negative refers to erosion and positive to deposition (a-c). The channel volumes below 0 m (d), −5 m (e) and −10 m (f) isobaths. Changes in channel volume from 1995 to 2007 (g) and from 2007 to 2018 (h), the orange curve shows the changes of channel volume from 1995 to 2018.

4. Results

4.1. Variations of erosion-deposition patterns associated with reclamations

Before the execution of a series of reclamation projects, between 1995 and 2007, there was area-integrated erosion observed in upper and middle segments and area-integrated deposition in the lower segment (Fig. 2a). The strongest amount of erosion (volume change of -1.5×10^7 m^3) occurred in 27–28 km downstream of the starting point of NC. The largest amount deposited (volume change of 3.6×10^6 m^3) occurred in 36–37 km downstream of the starting point (Fig. 2g).

In the upper segment, deposition mainly occurred on the shoal near the south bank, while erosion occurred in the channel along the north bank (Fig. 2a). The rates of volume change below the depth of 0 m and −5 m were -1.08×10^7 m^3 yr^{-1} and -1.07×10^7 m^3 yr^{-1}(Fig. 2d-e). In middle and lower segments, there was deposition on the shoal near the north bank, while erosion occurred in the channel along the south bank (Fig. 2a). In the middle segment, the rates of volume change below the depth of 0 m and −5 m were -5.75×10^6 m^3 yr^{-1} and -4.30×10^6 m^3 yr^{-1} (Fig. 2d-e), respectively. In the lower segment, the rates of volume change below the depth of 0 m and −5 m were -1.29×10^5 m^3 yr^{-1} and -1.07×10^6 m^3 yr^{-1} (Fig. 2d-e).

After the construction of the Qingcaosha Reservoir and HESP, from 2007 to 2018, the strongest erosion (volume change of 1.22×10^7 m^3) occurred in 41–42 km downstream of the starting point and deposition was the strongest (volume change of -4.43×10^6 m^3) in 37–38 km from the starting point (Fig. 2h).

Due to the construction of Qingcaosha Reservoir and the growth of its outer shoal (Fig. 2b), the rate of volume change below 0 m was 3.21×10^6 m^3 yr^{-1} in the upper segment (Fig. 2d). The volume change rate below a depth of −5 m was -3.97×10^6 m^3 yr^{-1} (Fig. 2e). The rate of volume changes below depth of 0 m and −5 m were -0.95×10^7 m^3 yr^{-1} and -1.13×10^7 m^3 yr^{-1} in the middle segment (Fig. 2d-e). The erosion rate of the channel below a depth of −5 m increased more than 150% after reclamations. Meanwhile, the lower segment transformed from a region of integrated deposition to one of integrated erosion (Fig. 2g-h). The erosion rate of the channel below a depth of −5 m increased more than 600% after reclamations. These findings provide support for the hypothesis that constructions of reclamations intensified the erosion in the channel. However, the volume below the depth of 0 m was 6.20×10^5 m^3 yr^{-1} (Fig. 2d) due to deposition of the tidal flat near the north bank (Fig. 2b). The volume change rate below the −5 m isobaths was -7.86×10^6 m^3 yr^{-1} (Fig. 2e). Furthermore, the volume change rate below the −10 m isobaths was -1.48×10^5 m^3 yr^{-1} (Fig. 2f).

4.2. Changes in the locations of boundaries of the TMZ

4.2.1. TMZ during spring tide

In 2006, the *ASSSC* of NC was 0.32 kg m^{-3} during spring tides in the dry season (Fig. 3a). The landward boundary of the TMZ was located at 121°52′ E (36 km to the begin point), the seaward boundary was at 122°12′ E (66 km to the begin point), the length of the TMZ was reduced to 30 km (Fig. 3d and g). After completion of the Qingcaosha Reservoir and the sixth phase of the HESP, the *ASSSC* reduced to 0.18 kgm^{-3} in 2011 (Fig. 3b). The landward boundary of the TMZ moved seawards by 9 km to 121°59 E, the seaward boundary of the TMZ moved seawards by 5 km to 122°14′ E and the length of the TMZ was 26 km (Fig. 3e and h). By 2019, the *ASSSC* decreased to 0.11 kg m^{-3} (Fig. 3c). The length of the TMZ was 24 km, with the landward boundary located at 121° 58 E and the seaward boundary located at 122° 12 E (Fig. 3f and i). The landward boundary moved landwards by 3 km, and the seaward boundary moved landwards by 5 km.

From 2006 to 2019, during spring tide, the landward boundary of the TMZ moved seaward by 6 km and the location of the seaward boundary presently wanders within a 3 km range from 122° 12′ E to 122° 14′ E.

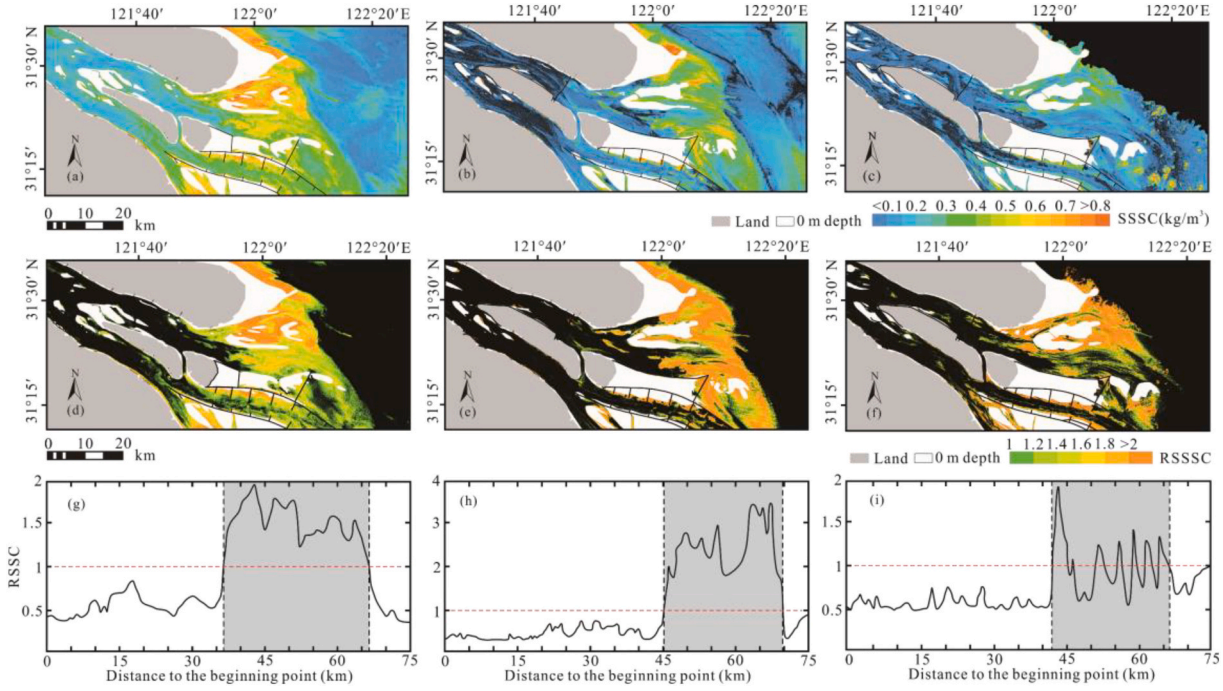

Fig. 3. The spatial distribution of surface suspended sediment concentration (SSSC) in the North Channel on 2006-11-06 (a), 2010-01-17 (b) and 2019-12-12 (c). Panels (d-f): as panels (a-c), but for the spatial distribution of the relative surface suspended sediment concentration (RSSSC). The RSSSC is the ratio of SSSC to region-averaged SSSC within the North Channel. Panels (g-i): the distribution of RSSSC along the longitudinal profile (the red line in Fig. 1c). The gray block indicates the turbidity maximum zone (where RSSSC >1). Left and right dashed lines were the landward boundary and seaward boundary of the turbidity maximum zone, respectively. (For interpretation of the references to colour in this figure legend, the reader is referred to the web version of this article.)

4.2.2. TMZ during neap tide

In 2006, the *ASSSC* of the NC was 0.15 kg m^{-3} (Fig. 4a), the landward boundary of the TMZ was 121°59 E (47 km to the begin point), the seaward boundary was 122°24′ E (84 km to the begin point) and the length of the TMZ was 37 km (Fig. 4d and g). In 2011, the *ASSSC* had decreased to 0.08 kg m^{-3} (Fig. 4b), the landward boundary of the TMZ had moved 5 km seawards to 122°3′ E, the seaward boundary of the TMZ had moved 2 km landwards to 122°23′ E and the extent of TMZ had shrunk to 33 km (Fig. 4e and h). By 2017, the *ASSSC* had decreased to 0.10 kg m^{-3} (Fig. 4c). The landward boundary had moved 12 km seawards to 122°9 E (Fig. 4f), but there was no change in the seaward boundary (Fig. 4i).

From 2006 to 2017, during neap tide, the landward boundary of the TMZ moved seaward by 17 km and the seaward boundary of the TMZ wandered in the range of 122° 23′ E to 122° 24′ E. The SSSC within the TMZ during neap tide was always lower than that during spring tide and the TMZ during neap tide was located downstream of that during spring tide.

4.3. Changes in the dominant flow

Before the execution of a series of reclamation projects, in 2003, the values of the dominant flow coefficient *R* values during spring tides at station BG1 were between 0.49 and 0.52 (Fig. 5a), so the stagnation point of near-bottom flow was closely located to this station. The values of *R* at station BG1 were 0.61 to 0.64 during neap tide, which showed that the ebb flow was dominant (Fig. 5a). In the lower segment, the values of *R* at station BG3 were between 0.49 and 0.52 during spring tide (Fig. 5b). During neap tide, the values of *R* below −0.5 depth were between 0.34 and 0.45, which shows that the flow was flood dominant (Fig. 5b). In addition, there was an obvious estuarine circulation at BG3 station.

After the construction of the Qingcaosha Reservoir and the EHSP, in 2018, values of the dominant flow coefficient *R* at station BG1 were between 0.68 and 0.71 during spring tide and between 0.76 and 0.78 during neap tide (Fig. 5c). Thus, with respect to earlier years, the ebb dominance increased. Values of *R* at station BG2 ranged from 0.63 to 0.65 during spring tide and 0.69 to 0.72 during neap tide (Fig. 5d). Although station BG4 was 9 km downstream of BG3, the values of *R* at this station were between 0.62 and 0.65 during spring tide and between 0.51 and 0.63 during neap tide (Fig. 5e). Conditions were ebb-dominant at three stations during spring tides and neap tides; the stagnation point moved to a location downstream of the station BG4.

4.4. Changes in the tidally averaged SSC

According to the in-situ observations in 2003 and 2018 (See Fig. 6), after construction of the Qingcaosha Reservoir and completion of the HESP, there was a decline of tidally averaged SSC within the NC. At station BG1, located in the upper segment, the depth-mean of tidally averaged SSC decreased from 0.34 kg m^{-3} to 0.22 kg m^{-3} over spring tide and from 0.12 kg m^{-3} to 0.18 kg m^{-3} over neap tide (Fig. 7a and d). At station BG2, located in the middle segment, the depth-mean of tidally averaged SSC decreased from 0.63 kg m^{-3} to 0.32 kg m^{-3} over spring tide and decreased from 0.26 kg m^{-3} to 0.19 kg m^{-3} over neap tide (Fig. 7b and e). In the lower segment, in 2003, the depth-mean of tidally averaged SSC at BG3 was 1.00 kg m^{-3} over the spring tide and 0.37 kg m^{-3} over neap tide (Fig. 7c). In 2018, the depth-mean of tidally averaged SSC of station BG4 was 0.82 kg m^{-3} over spring tide and 0.48 kg m^{-3} over neap tide (Fig. 7f).

In 2003, the tidally averaged SSC at station BG2 over spring tide was 0.32 kg m^{-3} in the surface layer and 1.07 kg m^{-3} in the bottom layer (Fig. 7b). The vertical profile of tidally averaged SSC over neap tide showed a two-layer structure, with values of 0.16 kg m^{-3} near the surface and 0.96 kg m^{-3} near the bottom layer (Fig. 7b). After the

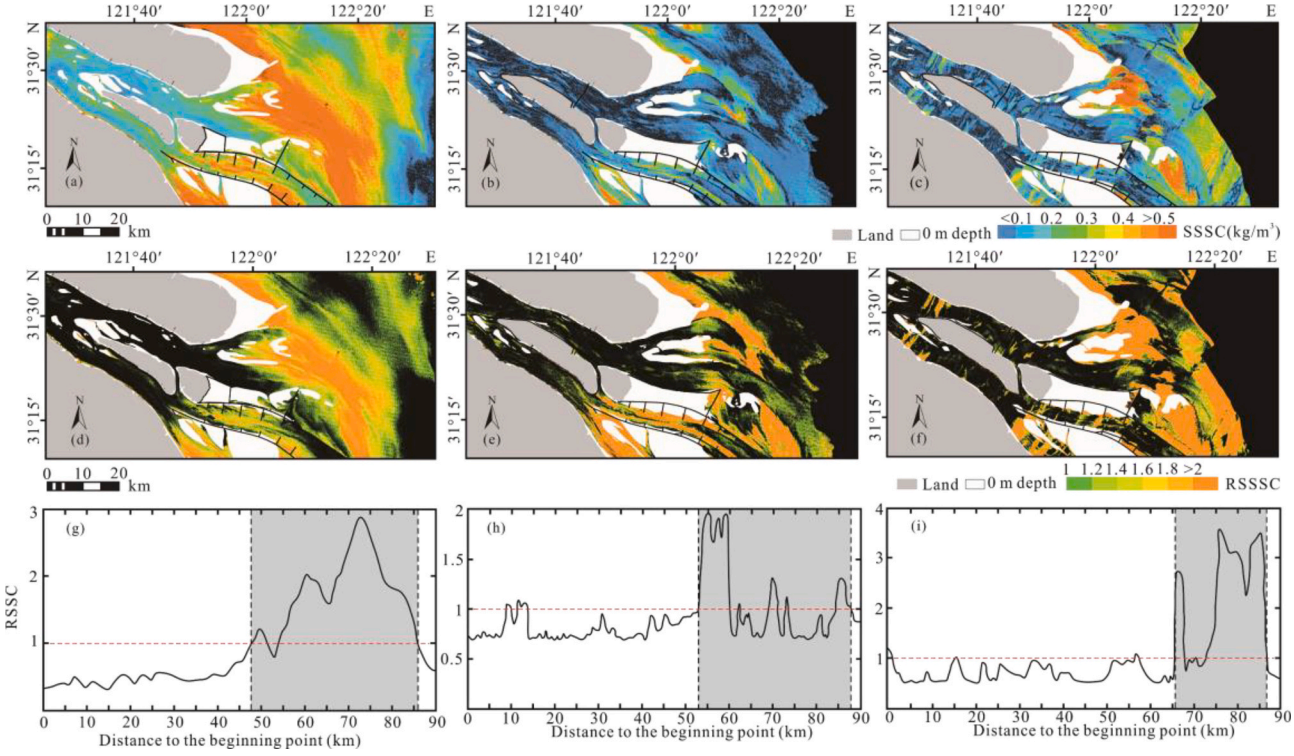

Fig. 4. The spatial distribution of surface suspended sediment concentration surface (SSSC) in the North Channel on 2006-01-22 (a), 2013-11-25 (b) and 2017-12-22 (c). Panels (d-f): as panels (a-c), but for the spatial distribution of the relative surface suspended sediment concentration (RSSSC). The RSSSC is the ratio of SSSC to region-averaged SSSC within the North Channel. Panels (g-i): the distribution of RSSSC along the longitudinal profile (the red line in Fig. 1c). The gray block indicates the turbidity maximum zone (where RSSSC >1). Left and right dashed lines were the landward boundary and seaward boundary of the turbidity maximum zone, respectively. (For interpretation of the references to colour in this figure legend, the reader is referred to the web version of this article.)

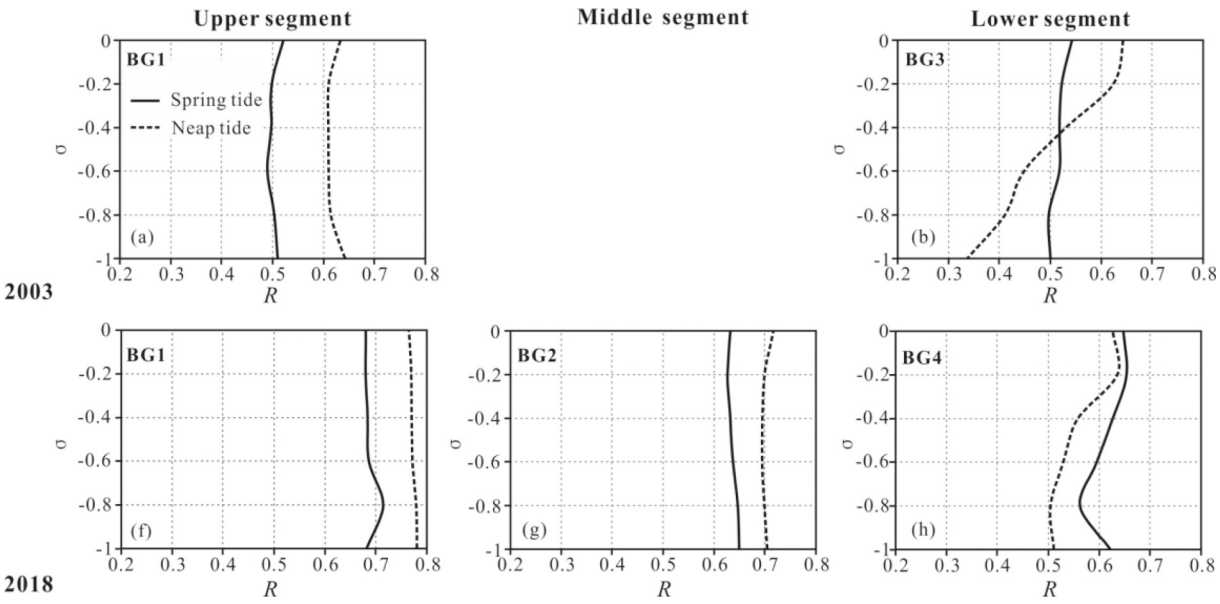

Fig. 5. Vertical profiles of the dominant flow coefficients R at stations BG1 (a) and BG2 (b) on 2003-02-18 (spring tide), 2003-02-24 (neap tide), at stations BG1 (c), BG2 (d) and BG4 (e) on 2018-04-18 (spring tide) and 2018–04-22 (neap tide). If $R > 0.5$ the flow is ebb-dominant, whereas if $R < 0.5$ the flow is flood-dominant. Here, σ is relative depth ($\sigma = 0$ is the surface and $\sigma = -1$ the bottom).

construction of a series of reclamation projects, the tidally averaged SSC near the bottom significantly decreased by 0.59 kg m^{-3} over the spring tide and 0.77 kg m^{-3} over neap tide (Fig. 7e). Therefore, in station BG2, where the landward boundary of the TMZ prior to the reclamations was located, the depth-mean tidally averaged SSC decreased significantly over the spring and neap tide.

4.5. Changes in characteristics of bed sediment

Measured data obtained in the dry season of 2003 showed that the median grain size of bed sediments was 126.2 μm and 16.5 μm in middle and lower segments, respectively (Liu et al., 2010). The measured data obtained in the dry season of 2018 showed that the bed sediment in the middle segment was silty sand with a median grain size of 178.8 μm, but the sediment in the lower segment was finer (sandy silt and silt with a median grain size of 18.2 μm). Coarser particles accounted for a large proportion of the sediment in all samples, as the skewness was negative. Thus, in the period 2003–2018, the bed sediment coarsened significantly in the middle segment. However, the change of the mean grain size of the surface sediment in the lower segment was small.

5. Discussion

5.1. Comparison with other estuaries

Land reclamations generally change the distribution of SSC, because they modify the morphology of an estuary. In e.g. the Ems estuary, located at the border between Germany and the Netherlands, it was found that the SSC increased due to the decrease in accommodation space for fine-grained sediments by land reclamations (van Maren et al., 2016). Constructions of land reclamations in Ribble estuary (van der Wal et al., 2002), Dee Estuary and Wash Estuary (Pye and Blott, 2014), all in the United Kingdom, reduced the tidal prism, leading to a reduction in average current speeds and accelerated sedimentation outside the embankments.

5.2. Changes in flow dominance and location of the stagnation point

The construction associated with the HESP fixed the southern boundary of the channel in the middle and lower segments. Therefore, the natural trend of the southward movement of the channel was limited. The reclamation intercepted flow and sediment exchange between the shoal and channel, which resulted in continuous erosion and an increase in the average water depth in the channel (Wu et al., 2016; Wei et al., 2017; Zhao et al., 2018). At the same time, deposition occurred near the northern band of the middle and lower segments. This happened because these areas were less affected by changes in the morphology and hydrodynamics of the channel and there was supply of offshore sediment (Zhu et al., 2016; Mei et al., 2018). The breadth-to-depth ratio B/H of the middle segment decreased from 1.20×10^3 to 1.06×10^3. That of the lower segment decreased from 5.67×10^3 to 3.69×10^3 (Table 4). The channel thus narrowed and deepened.

During the ebb tide, flow was concentrated within the deep channel. The numerical simulation results (Lyu and Zhu, 2019) showed that, after reclamations, the ratio of the water transport through NC to that through SB increased from 45% to 50%. Taking spring tide in the dry season as an example, the values of the dominant flow coefficient at station BG1 in 2003 was approximately 0.5 (Fig. 5a), so the stagnation point was located close to this station. However, flow at both BG1 and BG2 was obviously ebb dominant in 2018 (Fig. 5c and d), thereby revealing a downstream shift of the stagnation point. Numerical simulation results (Lyu and Zhu, 2019) showed that, after the constructions of reclamations, the salinity within channel on the south of the NC decreased in the dry season. Furthermore, the saline wedges moved seaward and the 5 PSU salinity isohaline moved to the middle of HESP at slack tide. Due to the estuarine circulation resulting from the longitudinal density gradient, a large amount of sediment was deposited in the TMZ, which occurred at the end of the salt tongue (Shen and Zhang, 1992). These findings explain the seaward shift of the landward boundary of the TMZ (Fig. 8).

5.3. Decline of tidally averaged SSC near the landward boundary of the TMZ

In the datasets of 2003 and 2018, variations of tidal ranges varied from 0.55 to 0.69 m (Table 3). They were less than variations of tidal ranges between spring and neap tide in the same year (1.07 m and 1.78 m, respectively). The effect of the tidal range on the vertical distribution of SSC could not be considered. Following an earlier study by Liu et al. (2014), the shape of the vertical profile of tidally averaged SSC was only

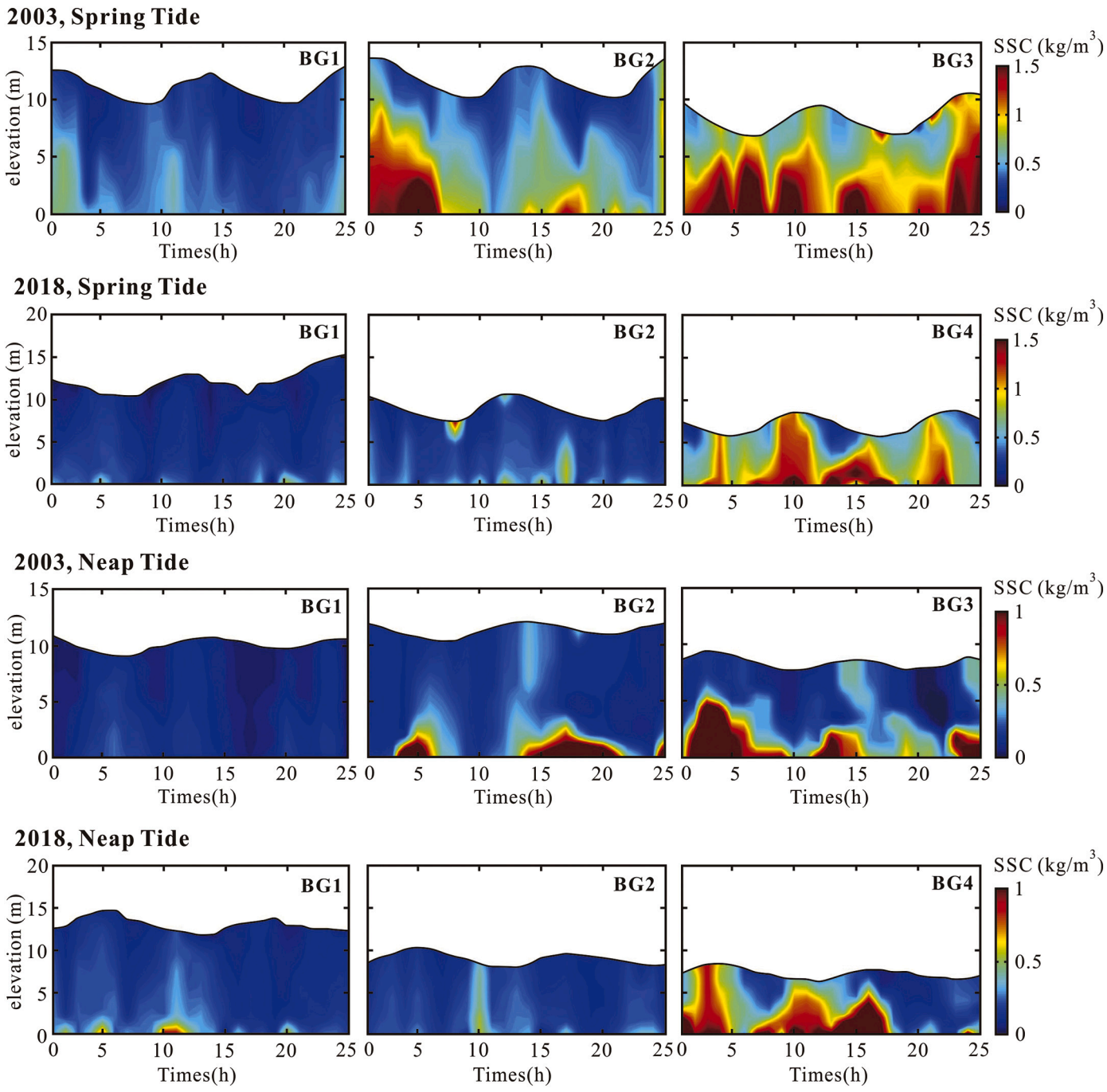

Fig. 6. Temporal variations of SSC (kg m^{-3}) at stations BG1 (a), BG2 (b), BG3 (c) on 2003-02-18 (spring tide), BG1 (d), BG2 (e), BG4 (f) on 2018-04-18 (spring tide), BG1 (g), BG2 (h), BG3 (i) on 2003-02-24 (neap tide), and BG1 (j), BG2 (k), BG4 (l) on 2018-04-22 (neap tide).

related to the dynamics of runoff, tide and the characteristics of surface sediments. The ratio of tidally averaged SSC in the surface and bottom layers were calculated to describe the shape of the vertical profile.

During spring tide, the ratio of tidally averaged SSC in the surface and bottom layers in BG2 decreased from 3.38 in 2003 to 1.74 in 2018 (Fig. 7b and e). During neap tide, the ratio of tidally averaged SSC in the surface and bottom layers in BG2 decreased from 6.11 in 2003 to 1.66 in 2018 (Fig. 7b and e). The tidally averaged SSC near the bottom decreased, which resulted in the decrease of the tidally averaged SSC in the middle segment.

This can be understood as follows. Owing to the enhancement of the ebb tide resulting from both the narrowing and fixing of channels associated with the reclamation projects and the interception of sediment flow from the shoal caused by the HESP, the source of fine-grained sediment in the deep channel has been reduced (Liu et al., 2014; Li et al., 2019). This resulted in the observed coarsening of surface sediments in the deep channel of the middle segment in the dry season, where also the landward boundary of the TMZ was located. From 2003 to 2015, in the flood season, the median particle size of surface sediments in the middle segment of NC increased from 127.4 μm to 193.94 μm (Liu et al., 2010; Li et al., 2019). This trend was similar to that during the dry season. The consequence was a weakening of the sediment resuspension. The tidally averaged SSC on the bottom at station BG2 in 2018 was significantly lower than that in 2003 and this led to a decline of the depth-mean of tidally averaged SSC at station BG2 (Fig. 7b and e). The landward boundary of the TMZ, which was in the 2 km seaward of

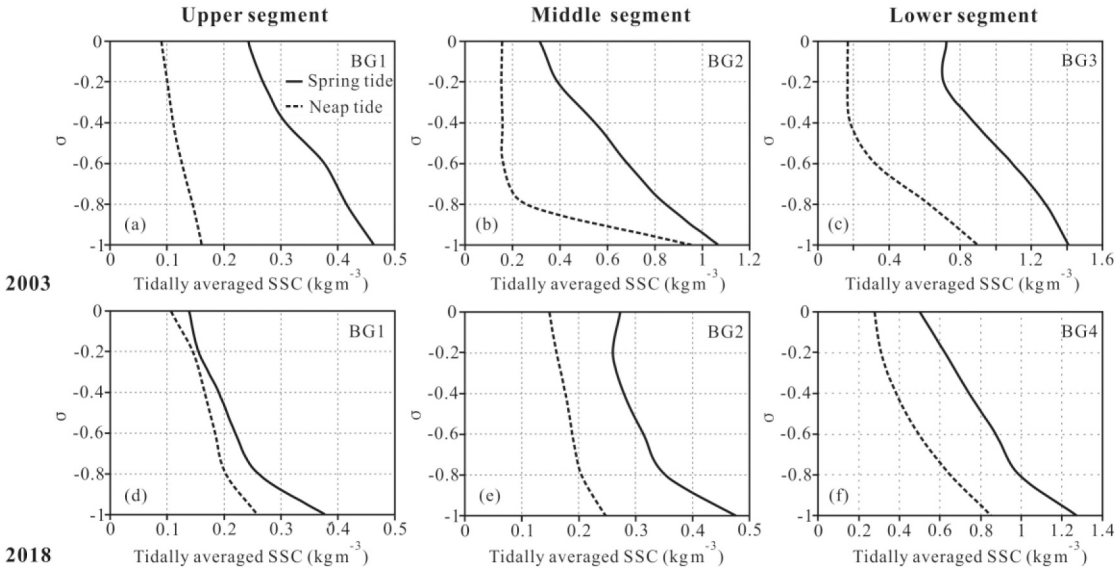

Fig. 7. Vertical profiles of tidally averaged suspended sediment concentrations at stations BG1 (a), BG2 (b), BG3 (c) on 2003-02-18 (spring tide), 2003-02-24 (neap tide), at stations BG1 (d), BG2 (e), BG4 (f) on 2018-04-18 (spring tide) and 2018-04-22 (neap tide) (d-f). Here, σ is relative depth ($\sigma = 0$ is the surface and $\sigma = -1$ the bottom).

Table 4
Average breadth and depth of NC in 1995, 2007and 2018.

	Average breadth B(km)			Average depth H (m)			B/H ($\times 10^3$)		
	1995	2007	2018	1995	2007	2018	1995	2007	2018
Upper segment	8.03	7.94	5.29	5.35	6.29	9.07	1.50	1.26	0.58
Middle segment	8.26	7.62	7.53	5.47	6.37	7.10	1.51	1.20	1.06
Lower segment	15.07	17.68	14.21	3.66	3.12	3.85	4.12	5.67	3.69

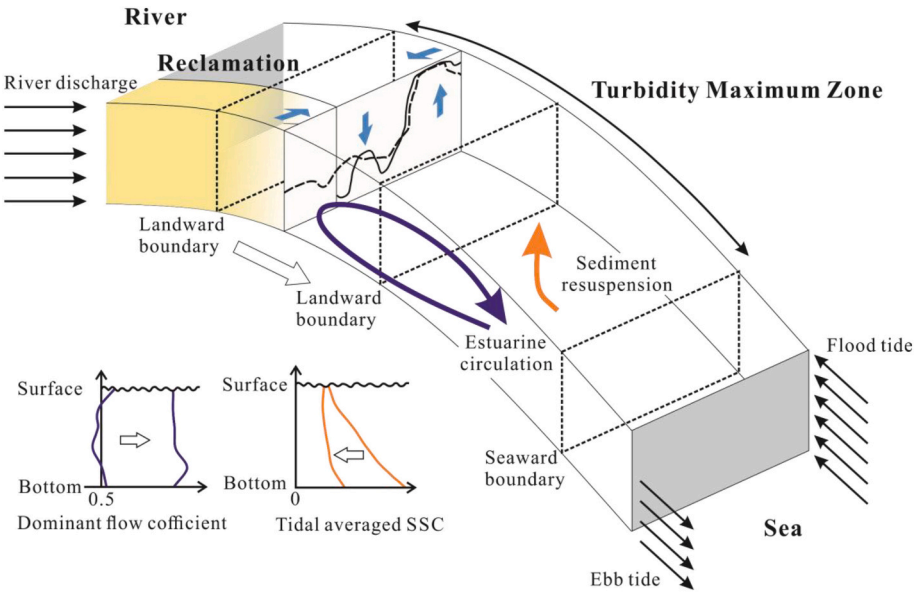

Fig. 8. A conceptual model of the shift of the turbidity maximum zone in response to reclamations. In the cross section of the channel, the solid line and dashed line are the channel bed before and after reclamations, respectively. The channel narrowed (blue horizontal arrow) and deepened (blue vertical arrow) as a result of reclamation works (yellow cube). This caused the coefficient of flow dominance to increase (purple curve in the first subpanel on the bottom left) and the estuarine circulation (purple arrow) area to move seaward. The sediment resuspension (orange arrow) decreased due to coarsening of surface sediment, the tidal average suspended sediment concentration (orange curve) on the bottom layer decreased (orange curve in the second subpanel on the bottom left) and the landward boundary of the turbidity maximum zone (the dash border) moved seaward. (For interpretation of the references to colour in this figure legend, the reader is referred to the web version of this article.)

station BG2, has moved 6 km seaward from the area. However, due to the replenishment of fine-grained sediment from the tidal flat and sea, the grain size of surface sediments in the lower segment is now finer (Zhu et al., 2016; Mei et al., 2018). The depth-mean of tidally averaged SSC of station BG4 (Fig. 7f), which was located near the core of the TMZ, has not significantly changed compared with that of BG3, which was also near the core of the TMZ (Fig. 7c).

A conceptual model of spatial changes in the TMZ in response to reclamation was proposed based on the above analysis (Fig. 8). In the middle segment, the deepened and narrowed channel caused by reclamations intensified the ebb-dominance and induced seaward migration of the stagnation point. In addition, surface sediment in the deep channel coarsened in response to the enhancement of ebb flow. The tidally averaged SSC near the bottom and the depth-mean of tidally

averaged SSC declined due to the decrease in resuspension. This all led to the seaward movement of the landward boundary of the TMZ. However, there were little variations in flow dominance and the characteristics of bed sediment in the outer estuary, which resulted from the strong tidal flow and replenishment of fine-grained sediment from the tidal flat and sea. Therefore, the seaward boundary of TMZ was less affected by reclamations.

An improvement with respect to previous studies (Jiang et al., 2013a, 2013b) is that we collected and compared remote sensing images for similar runoff and tidal conditions. This was done to exclude the impact of runoff and tides on the spatial distribution of surface suspended sediment concentration (SSSC). However, the number of images obtained with the same river discharge and tidal condition was limited, within the remote sensing images obtained by Landsat in the last two decades. Six images were retrieved at times that there were similar river discharges and tidal conditions, as well as few clouds. Furthermore, the construction of large-scale engineering works, such as the Three Gorges Dam, has resulted in a continuous reduction of SSSC in the Yangtze Estuary (YE). To avoid this effect on determining the characteristics of the TMZ, the SSSC was converted into RSSSC.

As a next step, it would be interesting to further quantify the influence of bathymetric configuration on estuarine circulation and sediment transport with a numerical model, but this is beyond the scope of the present study.

6. Conclusions

The key message of this study is that reclamation projects conducted in estuaries can cause dramatic changes in the geometry of channels and can thus affect the river and tidal flow and thereby cause spatial changes in the TMZ. This study focused on the NC of the YE, which has been strongly affected by reclamation in the past two decades. The main conclusions are listed below.

1) The narrowed and fixed channel caused by reclamation has induced erosion of the deeper channel and deposition on the tidal flat from 2007 to 2018. Erosion intensified below a depth of −5 m in middle and lower segments and the lower segment transformed from regions of net deposition to regions of net erosion. Deposition occurred on the shoal near the north bank in middle and lower segments. The average channel width decreased by 0.86–2.74 km, while the average depth increased by 0.19–3.72 m.
2) After construction of the large-scale reclamation projects, *ASSSC* within the TMZ in NC decreased during both spring tide and neap tide in the dry season. From 2006 to 2019, the landward boundary of the TMZ moved seaward by 6 km and the location of the seaward boundary presently wanders within a 3 km range from 122° 12′ E to 122° 14′ E during spring tide. The landward boundary of the TMZ moved seaward by 17 km and the seaward boundary of the TMZ wanders in the range of 122° 23′ to 122° 24′ during neap tide. The *SSSC* within the TMZ during neap tide is lower than that in spring tide and the TMZ during neap tide is located downstream of that during spring tide.
3) Ebb dominance enhanced due to deepening and narrowing of the channel that resulted from reclamations and this induced the seaward movement of the stagnation point that is located close to the core of the TMZ. In addition, bed sediment coarsened and its resuspension thus weakened. Consequently, the bottom tidally averaged SSC in the middle segment decreased by 0.59 kg m^{-3} during spring tide and 0.77 kg m^{-3} during neap tide, which resulted in a decline in the depth-mean of the tidally averaged SSC. All of these factors caused the landward boundary of the TMZ to move seawards.

Declaration of Competing Interest

None.

Acknowledgements

Thanks to Dr. Li Weihua and Dr. Zhang Erfeng, who led the in-situ observations. This work was supported by the National Natural Science Foundation of China-The Netherlands Organization for Scientific Research-Engineering and Physical Sciences Research Council (NSFC-NWO-EPSRC) (51761135023, EP/R02491X/1), the China Geological Survey (DD20190260) and the State Administration of Foreign Experts Affairs of China via the High-end Foreign Expert Project (G20200009096).

References

Burchard, H., Schuttelaars, H.M., Ralston, D.K., 2018. Sediment trapping in estuaries. Annu. Rev. Mar. Sci. 10, 371–395. https://doi.org/10.1146/annurev-marine-010816-060535.

Cheng, H.Q., Chen, J.Y., Chen, Z.J., Ruan, R.L., Xu, G.Q., Zeng, G., Zhu, J.R., Dai, Z.J., Chen, X.Y., Gu, S.H., Zhang, X.L., Wang, H.M., 2018. Mapping Sea level rise behavior in an estuarine delta system: a case study along the Shanghai coast. Engin. 4, 156–163. https://doi.org/10.1016/J.eng.2018.02.002.

Cheng, Z.X., Jalon, R.I., Wang, X.H., Liu, Y., 2020. Impacts of land reclamation on sediment transport and sedimentary environment in a macro-tidal estuary. Estuar. Coast. Shelf Sci. 242 https://doi.org/10.1016/j.ecss.2020.106861.

de Jonge, V.N., Schutterlaars, H.M., van Beusekom, J.E.E., Talke, S.A., de Swart, H.E., 2014. The influence of channel deepening on estuarine turbidity levels and dynamics, as exemplified by the Ems estuary. Estuar. Coast. Shelf Sci. 139, 46–59. https://doi.org/10.1016/j.ecss.2013.12.030.

Doxaran, D., Froidefond, J.M., Castaing, P., Babin, M., 2009. Dynamics of the turbidity maximum zone in a macrotidal estuary (the Gironde, France): Observations from field and MODIS satellite data. Estuar. Coast. Shelf Sci. 81, 321–332. https://doi.org/10.1016/j.ecss.2008.11.013.

Du, J.L., Yang, S.L., Feng, H., 2016. Recent human impacts on the morphological evolution of the Yangtze River delta foreland: a review and new perspectives. Estuar. Coast. Shelf Sci. 181, 160–169. https://doi.org/10.1016/j.ecss.2016.08.025.

Folk, R.L., Andrews, P.B., Lewis, D.W., 1970. Detrital sedimentary rock classification and nomenclature for use in New Zealand. New. Zeal. Geol. Geop. 13 (4), 937–968. https://doi.org/10.1080/00288306.1970.10418211.

Gao, G.D., Wang, X.H., Bao, X.W., Song, D.H., Lin, X.P., Qiao, L.L., 2018. The impacts of land reclamation on suspended-sediment dynamics in Jiaozhou Bay, Qingdao, China. Estuar. Coast. Shelf Sci. 206, 61–75. https://doi.org/10.1016/j.ecss.2017.01.012.

Gebhardt, A.C., Schoster, F., Gaye, H., Beeskow, B., Rachold, V., Unger, D., Ittekkot, V., 2005. The turbidity maximum zone of the Yenisei River (Siberia) and its impact on organic and inorganic proxies. Estuar. Coast. Shelf Sci. 65, 61–73. https://doi.org/10.1016/j.ecss.2005.05.007.

Guo, L.C., Su, N., Zhu, C.Y., He, Q., 2018. How have the river discharges and sediment loads changed in the Changjiang River basin downstream of the three Gorges Dam? J. Hydrol. 560, 259–274. https://doi.org/10.1016/j.jhydrol.2018.03.035.

Jiang, C.J., de Swart, H.E., Li, J.F., Liu, G.F., 2013a. Mechanisms of along-channel sediment transport in the North Passage of the Yangtze Estuary and their response to large-scale interventions. Ocean Dyn. 63, 283–305. https://doi.org/10.1007/s10236-013-0594-4.

Jiang, X.Z., Lu, B., He, Y.H., 2013b. Response of the turbidity maximum zone to fluctuations in sediment discharge from river to estuary in the Changjiang Estuary (China). Estuar. Coast. Shelf Sci. 131, 24–30. https://doi.org/10.1016/j.ecss.2013.07.003.

Lange, X., Burchard, H., 2019. The relative importance of wind straining and gravitational forcing in driving exchange flows in tidally energetic estuaries. J. Phys. Oceanogr. 49 (3), 723–736. https://doi.org/10.1175/JPO-D-18-0014.1.

Li, J.F., Zhang, C., 1998. Sediment resuspension and implications for turbidity maximum in the Changjiang Estuary. Mar. Geol. 148, 117–124. https://doi.org/10.1016/S0025-3227(98)00003-6.

Li, Z.H., Jia, J.J., Wu, Y.S., Zong, H.B., Zhang, G.A., Wang, Y.P., Yang, Y., Zhou, L., Gao, S., 2019. Vertical distributions of suspended sediment concentrations in the turbidity maximum zone of the periodically and partially stratified Changjiang Estuary. Estuar. Coasts 42, 1475–1490. https://doi.org/10.1007/s12237-019-00605-2.

Liu, H., He, Q., Wang, Z.B., Weltje, J.G., Zhang, J., 2010. Dynamics and spatial variability of near-bottom sediment exchange in the Yangtze Estuary, China. Estuar. Coast. Shelf Sci. 86, 322–330. https://doi.org/10.1016/j.ecss.2009.04.020.

Liu, J.H., Yang, S.L., Zhu, Q., Zhang, J., 2014. Controls on suspended sediment concentration profiles in the shallow and turbid Yangtze Estuary. Cont. Shelf Res. 90, 96–108. https://doi.org/10.1016/j.csr.2014.01.021.

Luan, H.L., Ding, P.X., Wang, Z.B., Ge, J.Z., Yang, S.L., 2016. Decadal morphological evolution of the Yangtze Estuary in response to river input changes and estuarine engineering projects. Geomorphology 265, 12–23. https://doi.org/10.1016/j.geomorph.2016.04.022.

Lyu, H.H., Zhu, J.R., 2019. Impacts of tidal flat reclamation on saltwater intrusion and freshwater resources in the Changjiang Estuary. J. Coast. Res. 35 (2), 314–321. https://doi.org/10.2112/JCOASTRES-D-18-00077.1.

Mei, X.F., Dai, Z.J., Wei, W., Li, W.H., Wang, J., Sheng, H., 2018. Secular bathymetric variations of the North Channel in the Changjiang (Yangtze) Estuary, China, 1880-

2013: Causes and effects. Geomorphology 303, 30–40. https://doi.org/10.1016/j.geomorph.2017.11.014.
Mitchell, S.B., 2013. Turbidity maxima in four macrotidal estuaries. Ocean Coast. Manag. 79, 62–69. https://doi.org/10.1016/j.ocecoaman.2012.05.030.
Pye, K., Blott, S.J., 2014. The geomorphology of UK estuaries: the role of geological controls, antecedent conditions and human activities. Estuar. Coast. Shelf Sci. 150, 196–214. https://doi.org/10.1016/j.ecss.2014.05.014.
Shen, H.T., Zhang, C.L., 1992. Mixing of salt water and fresh water in the Changjiang River estuary and its effects on suspended sediment. Chin. Geogr. Sci. 2, 373–381. https://doi.org/10.1007/BF02664568.
Shen, F., Zhou, Y.X., Li, J.F., He, Q., Verhoef, W., 2013. Remotely sensed variability of the suspended sediment concentration and its response to decreased river discharge in the Yangtze estuary and adjacent coast. Cont. Shelf Res. 69, 52–61. https://doi.org/10.1016/j.csr.2013.09.002.
van der Wal, D., Pye, K., Neal, A., 2002. Long-term morphological change in the Ribble Estuary, Northwest England. Mar. Geol. 189 (3–4), 249–266. https://doi.org/10.1016/S0025-3227(02)00476-0.
van Maren, D.S., Oost, A.P., Wang, Z.B., Vos, P.C., 2016. The effect of land reclamations and sediment extraction on the suspended sediment concentration in the Ems Estuary. Mar. Geol. 376, 147–157. https://doi.org/10.1016/j.margeo.2016.03.007.
Wackerman, C., Hayden, A., Jonik, J., 2017. Deriving spatial and temporal context for point measurements of suspended-sediment concentration using remote-sensing imagery in the Mekong Delta. Cont. Shelf Res. 147, 231–245. https://doi.org/10.1016/j.csr.2017.08.007.
Wang, Y.H., Dong, P., Oguchi, T., Chen, S.L., Shen, H.T., 2013. Long-term (1842–2006) morphological change and equilibrium state of the Changjiang (Yangtze) Estuary, China. Cont. Shelf Res. 56, 71–81. https://doi.org/10.1016/j.csr.2013.02.006.
Webster, R., Oliver, M.A., 2007. Geostatistics for Environmental Scientists: Second Edition. John Wiley & Sons, Ltd, Chichester, pp. 153–193. https://onlinelibrary.wiley.com/doi/book/10.1002/9780470517277.
Wei, W., Dai, Z.J., Mei, X.F., Liu, J.P., Gao, S., Li, S.S., 2017. Shoal morphodynamics of the Changjiang (Yangtze) estuary: Influences from river damming, estuarine hydraulic engineering and reclamation project. Mar. Geol. 386, 32–43. https://doi.org/10.1016/j.margeo.2017.02.013.
Williams, J., Lee, G.H., Shin, H.J., Dellapenna, T., 2015. Mechanism for sediment convergence in the anthropogenically altered microtidal Nakdong Estuary, South Korea. Mar. Geol. 369, 79–90. https://doi.org/10.1016/j.margeo.2015.08.004.
Wu, J.X., Liu, J.T., Wang, X., 2012. Sediment trapping of turbidity maxima in the Changjiang Estuary. Mar. Geol. 303-306, 14–25. https://doi.org/10.1016/j.margeo.2012.02.011.
Wu, S.H., Cheng, H.Q., Xu, Y.J., Li, J.F., Zheng, S.W., 2016. Decadal changes in bathymetry of the Yangtze River Estuary: Human impacts and potential saltwater intrusion. Estuar. Coast. Shelf Sci. 182, 158–169. https://doi.org/10.1016/j.ecss.2016.10.002.
Yang, S.L., Liu, Z., Dai, S.B., Gao, Z.X., Zhang, J., Wang, H.J., Luo, X.X., Wu, C.S., Zhang, Z., 2010. Temporal variations in water resources in the Yangtze River (Changjiang) over the Industrial Period, based on reconstruction of missing monthly discharges. Water Resour. Res. 46, W10516 https://doi.org/10.1029/2009WR008589.
Zhang, E.F., Gao, S., Savenjie, H.H.G., Si, C.Y., Cao, S., 2019. Saline water intrusion in relation to strong winds during winter cold outbreaks: North Branch of the Yangtze Estuary. J. Hydrol. 574, 1099–1109. https://doi.org/10.1016/j.jhydrol.2019.04.096.
Zhang, Y.Z., Chen, R.S., Wang, Y., 2020. Tendency of land reclamation in coastal areas of Shanghai from 1998 to 2015. Land Use Policy 91. https://doi.org/10.1016/j.landusepol.2019.104370.
Zhao, J., Guo, L.C., He, Q., Wang, Z.B., van Maren, D.S., Wang, X.Y., 2018. An analysis on half century morphological changes in the Changjiang Estuary: Spatial variability under natural processes and human intervention. J. Mar. Syst. 181, 25–36. https://doi.org/10.1016/j.jmarsys.2018.01.007.
Zheng, S.W., Cheng, H.Q., Shi, S.Y., Xu, W., Zhou, Q.P., Jiang, Y.H., Zhou, F.N., Cao, M.X., 2018. Impact of anthropogenic drivers on subaqueous topographical change in the Datong to Xuliujing reach of the Yangtze River. Sci. China Earth Sci. 61, 940–950. https://doi.org/10.1007/s11430-017-9169-4.
Zhu, L., He, Q., Shen, J., Wang, Y., 2016. The influence of human activities on morphodynamics and alteration of sediment source and sink in the Changjiang Estuary. Geomorphology 273, 52–62. https://doi.org/10.1016/j.geomorph.2016.07.025.